Inorg. Chem. **2003**, *42*, 5890–5899

Equilibria between Metallosupramolecular Squares and Triangles with the New Rigid Linker 1,4-Bis(4-pyridyl)tetrafluorobenzene. Experimental and Theoretical Study of the Structural Dependence of NMR Data

Montserrat Ferrer,*,† Mounia Mounir,† Oriol Rossell,† Eliseo Ruiz,† and Miguel Angel Maestro‡

Departament de Química Inorgànica, Universitat de Barcelona, Martí i Franquès 1-11, 08028 Barcelona, Spain, and Servicios Xerais de Apoio à Investigacion, Universidade da Coruña, Edificio anexo Facultad de Ciencias, Campus de Zapateira, s/n, 15071 A Coruña, Spain

Received May 9, 2003

The new fluorinated rigid ligand **L**, 1,4-bis(4-pyridyl)tetrafluorobenzene, was used in combination with different diphosphine Pd(II) and Pt(II) triflates to build metallosupramolecular assemblies. Complex equilibria between triangular and square entities were detected for all the cases. Characterization of the equilibria was accomplished by ^{1}H, ^{31}P{^{1}H}, ^{19}F, and ^{195}Pt{^{1}H} NMR in combination with mass spectrometry. The square/triangle ratio was seen to depend on several factors, such as the nature of the metal corners, the concentration, and the solvent. The relative stability of the square and triangular complexes was explored by using force field methods. A GIAO-DFT study was carried out to analyze the changes of the ^{31}P and ^{1}H NMR data with the geometry of the complexes.

Introduction

Transition-metal-directed self-assembly has for some time been used to construct various types of supramolecular polygons such as triangles, squares and rectangles, pentagons and hexagons, and more complex structures.[1] The introduction of functionality into these systems, such as redox-activity,[2] magnetic,[3] or luminiscence properties[4,5] is one of the major current research areas in supramolecular chemistry. By far, self-assembled squares or rectangles have been the most studied molecules, and although the majority of them are based on the square-planar geometry of Pt(II) or Pd (II) complexes,[6] there are a few reported examples of molecular squares based on an octahedral geometry at the metal center.[5,7c,d] Notably, molecular squares usually bear highly positive charges, and could thus be potential hosts for electron-rich species.[8] In sharp contrast to the numerous examples of square or rectangular structures reported, triangular complexes are much less common, mainly due to the scarcity of suitable building blocks with proper turning angles.[1] Nevertheless, in some cases, triangular structures

* To whom correspondence should be addressed. E-mail: montse.ferrer@qi.ub.es.
† Universitat de Barcelona.
‡ Universidade da Coruña.

(1) (a) Leininger, S.; Olenyuk, B.; Stang P. J. *Chem. Rev.* **2000**, *100*, 853−908. (b) Fujita, M. *Chem. Soc. Rev.* **1998**, *27*, 417−425. (c) Swiegers, G. F.; Malefetse, T. J. *Chem. Rev.* **2000**, *100*, 3483−3537. (d) Holliday, J. H.; Mirkin, C. A. *Angew. Chem., Int. Ed.* **2001**, *40*, 2022−2043.
(2) McQuillan, F. S.; Berridge, T. G.; Chen, H.; Hamor, T. A.; Jones, C. J. *Inorg. Chem.* **1998**, *37*, 4959−4970.
(3) Solari, E.; Lesueuer, W.; Klose, A.; Schenk, K.; Floriani, C.; Chiesi-Vila, A.; Rizzoli, C. *J. Chem. Soc., Chem. Commun.* **1996**, 807−808.
(4) (a) Slone, R. V.; Hupp, J. T.; Stern, C. L.; Albrecht-Schmitt, T. E. *Inorg. Chem.* **1996**, *35*, 4096−4097. (b) Slone, R. V.; Hupp, J. T. *Inorg. Chem.* **1997**, *36*, 5422−5423. (c) Slone, R. V.; Benkstein, K. D.; Belanger, S.; Hupp, J. T.; Guzei, I. A.; Rheingold, A. L. *Coord. Chem. Rev.* **1998**, *171*, 221−243. (d) Belanger, S.; Hupp, J. T.; Stern, C. L.; Slone, R. V.; Watson, D. F.; Carrell T. G. *J. Am. Chem. Soc.* **1999**, *121*, 557−563.
(5) Sun, S.-S.; Lees, A. J. *Coord. Chem. Rev.* **2002**, *230*, 171−192.
(6) See, for example: (a) Fujita, M.; Yazaki, J.; Ogura, K. *J. Am. Chem. Soc.* **1990**, *112*, 5645−5647. (b) Fujita, M.; Yazaki, J.; Ogura, K. *Tetrahedron Lett.* **1991**, *32*, 5589−5592. (c) Fujita, M.; Nagao, S.; Iida, M.; Ogura, K. *J. Am. Chem. Soc.* **1993**, *115*, 1574−1576. (d) Stang P. J.; Cao, D. H. *J. Am. Chem. Soc.* **1994**, *116*, 4981−4982. (e) Manna, J.; Kuehl, C. J.; Whiteford, J. A.; Stang, P. J.; Muddiman, D. C.; Hofstadler, S. A.; Smith, R. D. *J. Am. Chem. Soc.* **1997**, *119*, 11611−11619. (f) Zhang, Y.; Wang, S.; Enright, G. D.; Breeze, S. R. *J. Am. Chem. Soc.* **1998**, *120*, 9398−9399. (g) Onitsuka, K.; Yamamoto, S.; Takahashi, S. *Angew. Chem., Int. Ed.* **1999**, *38*, 174−176.
(7) (a) Cotton, F. A.; Daniels, L. M.; Lin, C.; Murillo, C. A. *J. Am. Chem. Soc.* **1999**, *121*, 4538−4539. (b) Fujita, M.; Aoyagi, M.; Ogura, K. *Inorg. Chim. Acta* **1996**, *246*, 53−57. (c) Sun, S.-S.; Lees, A. J. *Inorg. Chem.* **1999**, *38*, 4181−4182. (d) Sun, S.-S.; Lees, A. J. *J. Am. Chem. Soc.* **2000**, *122*, 8956−8967 (e) Schnebeck, R.-D.; Freisinger E.; Lippert, B. *Angew. Chem., Int. Ed.* **1998**, *37*, 119−123. (f) Schnebeck, R.-D.; Freisinger, E.; Glahe, F.; Lippert, B. *J. Am. Chem. Soc.* **2000**, *122*, 1381−1390. (g) Lai, S.-W.; Chan, M. C.-W.; Peng, S.-M.; Che, C.-M. *Angew. Chem., Int. Ed.* **1999**, *38*, 669−671. (h) Schweiger, M.; Seidel, S. R.; Arif, A. M.; Stang, P. J. *Angew. Chem., Int. Ed.* **2001**, *40*, 3467−3469.
(8) Stang, P. J.; Fan, J.; Olenyuk, B. *Acc. Chem. Res.* **1997**, *30*, 502−518 and references therein.

10.1021/ic034489j CCC: $25.00
Published on Web 08/06/2003

have been obtained by carefully adjusting the experimental conditions and choosing the appropriate bridging ligand;[7] for example, generally, less rigid building blocks favor the self-assembly of triangular supramolecules. It has been suggested that the driving force for the self-assembly process is under thermodynamic control:[9] molecular squares are less strained and hence more stable in terms of enthalpy, while entropic factors favor the triangle since it is assembled from a smaller number of units. Recently, however, the stoichiometric combination of ≈90° corners with several linear linking units has led to a mixture of triangular and square entities in equilibrium,[10] demonstrating that the two products are close together in energy and consequently the self-assembly reactions are not yet as predictable to the same degree as classical reaction sequences. This equilibrium tends to be concentration dependent, that is, at higher concentration, the equilibrium shifts significantly in the direction of the molecular square producing three molecules from four of the molecular triangles. In addition, trimeric or tetrameric assemblies are clearly induced by the presence of appropriate guests.[10c] We note that Stang et al. have just proved that the selective crystallization of either of the two species can be accomplished by the appropriate choice of solvents and ratio of anions present in the system.[11] The present paper reports the preparation and characterization of a series of *cis*-diphosphine-Pt(II)- or -Pd(II)-based self-assembly macrocyclic compounds with the new fluorinated ligand 1,4-bis(4-pyridyl)tetrafluorobenzene **L**. Formation of triangle−square equilibria was observed in all cases. The compositions of these equilibria have been studied by multinuclear NMR spectroscopy and mass spectrometry with the result that the molecular square is the major component for diphosphine = dppp, 1,3-bis(diphenylphosphino)propane, while the molecular triangle is the major component in the case of diphosphine = dppf, 1,1′-bis(diphenylphosphino)ferrocene. For the case of diphosphine = depe, 1,2-bis(diethylphosphino)ethane, a more complex behavior was observed.

Experimental Section

General Procedures. All manipulations were performed under prepurified N_2 using standard Schlenk techniques. All solvents were distilled from appropriate drying agents. Commercial reagents 4-bromopyridine hydrochloride, 1,4-dibromotetrafluorobenzene, dppp, depe, and dppf were used as received. The compounds $[Pd(PPh_3)_4]$,[12] $[PtCl_2(COD)]$,[13] $[PdCl_2(COD)]$,[14] $[Pt(dppp)(H_2O)_2](OTf)_2$,[15] $[Pd(dppp)(H_2O)_2](OTf)_2$,[15] $[Pt(dppf)(H_2O)_2](OTf)_2$,[16a] and $[Pd(dppf)(H_2O)_2](OTf)_2$[16a] were prepared as described previously.

Physical Measurements. Infrared spectra were recorded on a FT-IR 520 Nicolet spectrophotometer. $^{31}P\{^1H\}$ NMR (δ(85% H_3PO_4) = 0.0 ppm), $^{195}Pt\{^1H\}$ NMR (δ (35% $K_2[PtCl_6]$) = 0.0 ppm), ^1H NMR (δ(TMS) = 0.0 ppm), ^{13}C NMR (δ(TMS) = 0.0 ppm) and ^{19}F NMR ($\delta(CFCl_3)$ = 0.0 ppm) spectra were obtained on a Bruker DXR 250 and Varian 300 and 200 spectrometers at 25 °C unless otherwise stated. Elemental analyses of C, H, N, and S were carried out at the Serveis Científico-Tècnics in Barcelona. FAB(+) and electrospray mass spectra were recorded from concentrated solutions of the products on a Fisions VG Quattro spectrometer.

Electrochemical measurements for the dppf complexes were recorded on a Princeton Applied Research model 263A potentiostat (EG&G instruments). The electrochemical cell consisted of a platinum disk working electrode (TACUSSEL-EDI rotatory electrode (3.14 mm^2)), a platinum wire auxiliary electrode, and a Ag/$AgNO_3$ (0.1 M, in acetonitrile solution) reference electrode separated from the solution by a medium-porosity fritted disk. Cyclic voltammograms were obtained from 5×10^{-4} M solutions of the samples under nitrogen at 25 °C using dry CH_2Cl_2 as solvent and tetrabutylammonium hexafluorophosphate (0.1 M) as supporting electrolyte. For electrolysis experiments a Pt gauze was used. Ferrocene (Fc) was used as an internal reference with the redox couple Fc/Fc^+ occurring at 0.15 V.

Computational Details. Force field calculations using the Universal force field[17] with the Cerius2 package[18] were used to determine the optimal conformation of the studied complexes. Several conformer searches and molecular dynamics studies have been performed using different algorithms in order to reach the lowest-energy conformer for each complex.

The calculation of the shielding shifts was carried out using the GIAO (gauge invariant atomic orbital) method[19,20] implemented in the Gaussian98 code.[21] The calculations were performed using the hybrid B3LYP functional[22−24] and the Stoll−Preuss pseudopoten-

(9) Chi, X.; Guerin, A. J.; Haycock, R. A.; Hunter, C. A.; Sarson, L. D. *J. Chem. Soc., Chem. Commun.* **1995**, 2563−2565.

(10) (a) Fujita, M.; Sasaki, O.; Mitsuhashi, T.; Fujita, T.; Yazaki, J.; Yamaguchi, K.; Ogura, K. *J. Chem. Soc., Chem. Commun*. **1996**, 1535−1536. (b) Fujita, M.; Ogura, K. *Coord. Chem. Rev*. **1996**, *148*, 249−264. (c) Fujita, M.; Ogura, K. *Bull. Chem. Soc. Jpn*. **1996**, *69*, 1471−1482. (d) Lee, S. B.; Hwang, S.; Chung, D. S.; Yun, H.; Hong, J.-I. *Tetrahedron Lett*. **1998**, *39*, 873−876. (e) Romero, F. M.; Ziessel, R.; Dupont-Gervais, A.; van Dorsselaer, A. *J. Chem. Soc., Chem. Commun*. **1996**, 551−553. (f) Schnebeck, R.-D.; Freisinger, E.; Lippert, B. *Eur. J. Inorg. Chem*. **2000**, 1193−1200. (g) Sautter, A.; Schmid, D. G.; Jung, G.; Würthner, F. *J. Am. Chem. Soc*, **2001**, *123*, 5424−5430 (h) Park, K.-M.; Kim, S.-Y.; Heo, J.; Whang, D.; Sakamoto, S.; Yamaguchi, K.; Kim, K. *J. Am. Chem. Soc*. **2002**, *124*, 2140−2147.

(11) Schweiger, M.; Seidel, S. R.; Arif, A. M.; Stang, P. J. *Inorg. Chem*. **2002**, *41*, 2556−2559.

(12) Coulson, D. R. *Inorg. Synth*. **1972**, *13*, 121−124.

(13) McDermott, J. X.; White, J. F.; Whitesides, G. M. *J. Am Chem. Soc*. **1976**, *98*, 6521−6528.

(14) Drew, D.; Doyle, J. R. *Inorg. Synth*. **1990**, *28*, 346−349.

(15) Stang, P. J.; Cao, D. H.; Saito, S.; Arif, A. M. *J. Am. Chem. Soc*. **1995**, *117*, 6273−6283.

(16) (a) Stang, P. J.; Olenyuk, B.; Fan, J.; Arif, A. M. *Organometallics* **1996**, *15*, 904−908. (b) Sun, S.-S.; Anspach, J. A.; Lees, A. J. *Inorg. Chem.* **2002**, *41*, 1862−1869.

(17) Rappe, A. K.; Casewit, C. J.; Colwell, K. S.; Goddard, W. A., III; Skiff, W. M. *J. Am. Chem. Soc.* **1992**, *114*, 10024−10035.

(18) *Cerius2*, version 3.8; Molecular Simulations: San Diego, 1998.

(19) Wolinski, K.; Hinton, J. F.; Pulay, P. J. *J. Am. Chem. Soc.* **1990**, *112*, 8251−8260.

(20) Ditchfield, R. *Mol. Phys.* **1974**, *27*, 789−807.

(21) Frisch, M. J.; Trucks, G. W.; Schlegel, H. B.; Scuseria, G. E.; Robb, M. A.; Cheeseman, J. R.; Zakrzewski, V. G.; Montgomery, J. A.; Stratmann, R. E.; Burant, J. C.; Dapprich, S.; Millam, J. M.; Daniels, A. D.; Kudin, K. N.; Strain, M. C.; Farkas, O.; Tomasi, J.; Barone, V.; Cossi, M.; Cammi, R.; Mennucci, B.; Pomelli, C.; Adamo, C.; Clifford, S.; Ochterski, J.; Petersson, G. A.; Ayala, P. Y.; Cui, Q.; Morokuma, K.; Malick, D. K.; Rabuck, A. D.; Raghavachari, K.; Foresman, J. B.; Cioslowski, J.; Ortiz, J. V.; Stefanov, B. B.; Liu, G.; Liashenko, A.; Piskorz, P.; Komaromi, I.; Gomperts, R.; Martin, R. L.; Fox, D. J.; Keith, T.; Al-Laham, M. A.; Peng, C. Y.; Nanayakkara, A.; Gonzalez, C.; Challacombe, M.; Gill, P. M. W.; Johnson, B. G.; Chen, W.; Wong, M. W.; Andres, J. L.; Head-Gordon, M.; Replogle, E. S.; Pople, J. A. *GAUSSIAN98 (A.11)*; Gaussian, Inc.: Pittsburgh, PA, 1998.

(22) Becke, A. D. *J. Chem. Phys.* **1993**, *98*, 5648−5652.

(23) Becke, A. D. *Phys. Rev. A* **1988**, *38*, 3098−3100.

(24) Lee, C.; Yang, W.; Parr, R. G. *Phys. Rev. B* **1988**, *37*, 785−789.

tials[25] for the metal atoms while the IGLO-II basis set[26] was employed for the main group elements. We employed a 6-31G* basis set[27] for the geometry optimizations of the complexes. The relativistic contributions seem to be important for the estimation of the chemical shift of complexes with heavy transition metals. However, some authors have seen that for heavy metals the use of the relativistic pseudopotentials provides good estimates of the shielding shift of the neighbor atom.[28,29]

1,4-Bis(4-pyridyl)tetrafluorobenzene (L). To 3.90 mmol of 4-bromopyridine prepared from 758 mg (3.90 mmol) of 4-bromopyridine hydrochloride[30] was added a THF solution (150 mL) containing 1.62 mmol of the Grignard reagent 1,4-dibromotetrafluorophenyldimagnesium followed by 450 mg (0.39 mmol) of [$Pd(PPh_3)_4$]. After 48 h of reaction at room temperature the mixture was treated with 50 mL of H_2O. The organic phase was removed, and the aqueous layer was extracted with CH_2Cl_2 (3 × 50 mL). The combined organic layers were dried (Na_2SO_4) and concentrated under reduced pressure until a beige precipitate was formed. The solid was purified by column chromatography on silica gel using first CH_2Cl_2 and subsequently CH_2Cl_2/CH_3OH (100:2) as eluent giving 187 mg (38% yield) of **L** as a white solid. Temperature of decomposition: 270−275 °C. ^{1}H NMR (250.13 MHz, $CDCl_3$): 8.81 (d-like, J = 5.1 Hz, 4H$_{\alpha-py}$), 7.46 (d-like, J = 5.1 Hz, 4H$_{\beta-py}$). ^{13}C NMR (62.89 MHz, $CDCl_3$): 150.3 (C$_{\alpha-py}$), 144.1 (dm, $^1J_{C-F}$ = 259 Hz, C−F), 135.2 (C$_{\gamma-py}$), 130.3 (m, C$_q$), 124.5 (C$_{\beta-py}$). ^{19}F NMR (282.21 MHz, $CDCl_3$): −146.4 (s). Anal. Calcd for $C_{16}H_8F_4N_2$: C, 63.16; H, 2.65; N, 9.21. Found: C, 62.99; H, 2.64; N, 8.98. IR (KBr, cm^{-1}): 1595 (C−N), 1467 (C═C), 981 (C−F), 822 (C−H). MS (IE) *m*/*z*: 305 (M + 1)$^+$, 304 (M)$^+$, 285 (M − 19)$^+$.

[**Pt(OTf)$_2$(depe)] (1c).** The precursor [$PtCl_2$(depe)] was obtained by dropwise addition of a CH_2Cl_2 (10 mL) solution of 0.3 mL (1.34 mmol) of depe[31] to 500 mg (1.34 mmol) of [$PtCl_2$(COD)] in 60 mL of the same solvent. After 1 h of reaction at room temperature the mixture was concentrated to half volume and Et_2O was added to precipitate a yellowish solid, which was purified by recrystallization (CH_2Cl_2/Et_2O), giving pure [$PtCl_2$(depe)], 380 mg (60% yield). ^{1}H NMR (250.13 MHz, $CDCl_3$): 2.13 (dm, 8H, −CH*$_2$−CH$_3$), 1.85 (m, 4H, −P−CH$_2$−CH$_2$−P−), 1.23 (dt, $^3J_{H-P}$ = 22.1 Hz, $^3J_{H-H}$ = 7.6 Hz, 12H, −CH$_3$). ^{31}P{^{1}H} NMR (101.25 MHz, $CDCl_3$): 57.2 (s, J_{P-Pt} = 3545 Hz). Anal. Calcd for $C_{10}H_{24}Cl_2P_2Pt$: C, 25.43; H, 5.12. Found: C, 25.48; H, 5.13.

1c was synthesized by addition of 350 mg (1.36 mmol) of solid AgOTf to a CH_2Cl_2 (50 mL) solution of 215 mg (0.45 mmol) of [$PtCl_2$(depe)]. The reaction mixture was stirred for 3 h with exclusion of light. After filtration, the resulting solution was concentrated to 10 mL in vacuo and an off-white solid was precipitated upon addition of 20 mL of Et_2O. Subsequent recrystallization (CH_2Cl_2/Et_2O) gave 94 mg (30%) of pure **1c**.^{1}H NMR (250.13 MHz, CD_2Cl_2): 2.22 (dm, 8H, P−CH*$_2$−CH$_3$), 1.95 (m, 4H, −P−CH$_2$−CH$_2$−P−), 1.30 (dt, $^3J_{H-P}$ = 19.7 Hz, $^3J_{H-H}$ = 7.6 Hz, 12 H, −CH$_3$). ^{31}P{^{1}H} NMR (101.25 MHz, CD_2Cl_2): 54.9 (s, J_{P-Pt} = 3950 Hz). Anal. Calcd for $C_{12}H_{24}F_6O_6P_2PtS_2$: C, 20.61; H, 3.46; S, 9.17. Found: C, 20.65; H, 3.45; S, 9.13. IR (KBr, cm^{-1}): 2966, 2933, 2910, 2868 (depe), 1270, 1034, 641, 519 (OTf).

[**Pd(OTf)$_2$(depe)] (2c).** Experimental details for the synthesis of **1c** also apply for **2c** except that acetone was used as a solvent in the preparation of the precursor [$PdCl_2$(depe)]. Yield: 38%. ^{1}H NMR (250.13 MHz, C_2D_6CO): 2.66 (m, 4H, −P−CH$_2$−CH$_2$−P−), 2.40 (m, 8H, P−CH*$_2$−CH$_3$), 1.41 (dt, $^3J_{H-P}$ = 19.8 Hz, $^3J_{H-H}$ = 7.6 Hz, 12 H, −CH$_3$). ^{31}P{^{1}H} NMR(101.25 MHz, CH_2Cl_2, coaxial tube of 1% $P(OCH_3)_3$ in C_2D_6CO) 94.2 (s). Anal. Calcd for $C_{12}H_{24}F_6O_6P_2PdS_2$: C, 23.60; H, 3.96; S, 10.50. Found: C, 23.64; H, 3.94; S, 10.46. IR (KBr, cm^{-1}) 2970, 2930, 2900, 2870 (depe), 1260, 1027, 640, 517 (OTf).

Characterization data for [$PdCl_2$(depe)] (yield 65%): ^{1}H NMR (250.13 MHz, $CDCl_3$) 2.25 (dm, 8H, −CH*$_2$−CH$_3$), 2.04 (m, 4H, −P−CH$_2$−CH$_2$−P−), 1.30 (dt, $^3J_{H-P}$ = 18.9 Hz, $^3J_{H-H}$ = 7.6 Hz, 12H, −CH$_3$); ^{31}P{^{1}H} NMR(101.25 MHz, $CDCl_3$) 85.3 (s). Anal. Calcd for $C_{10}H_{24}Cl_2P_2Pd$: C, 31.31; H, 6.31. Found: C, 31.27; H, 6.29.

Square/Triangle 3a/3a′. Solid 1,4-bis(4-pyridyl)tetrafluorobenzene (**L**) (7 mg, 0.023 mmol) was added to a CH_3NO_2 (3 mL) solution of [$Pt(dppp)(H_2O)_2$]$(OTf)_2$ (**1a**) (21 mg, 0.023 mmol) at room temperature. After 3 h of stirring, the reaction mixture was concentrated to 1.5 mL under reduced pressure and a white solid was precipitated upon addition of 15 mL of Et_2O. Filtration and drying in vacuo gave 22 mg (78%) of the product. **3a**: ^{1}H NMR (250.13 MHz, CD_3NO_2) 8.93 (d-like, J = 5.0 Hz, 16H, H$_{\alpha-py}$), 7.76−7.35 (m, 80H, Ph), 7.34 (d-like, J = 5.0 Hz, 16H, H$_{\beta-py}$), 3.35 (brs, 16H, −P−CH*$_2$−CH$_2$−CH*$_2$−P−), 2.41 (m, 8H, −P−CH$_2$−CH*$_2$−CH$_2$−P−); ^{31}P{^{1}H} NMR (101.25 MHz, CD_3NO_2); −14.8 (s, J_{Pt-P} = 3001 Hz); ^{19}F NMR (282.21 MHz, CH_3NO_2, coaxial tube of CF_3COOH in D_2O) −81.3 (s, 24F, OTf), −145.3 (s, 16F, F$_L$); ^{195}Pt{^{1}H} NMR (53.53 MHz, CD_3NO_2) −4434 (t, J_{Pt-P} = 3001 Hz). **3a′**: ^{1}H NMR (250.13 MHz, CD_3NO_2) 8.78 (d-like, J = 4.9 Hz, 12H, H$_{\alpha-py}$), 7.76−7.35 (m, 60H, Ph), 7.30 (d-like, J = 4.9 Hz, 12H, H$_{\beta-py}$), 3.35 (brs, 12H, −P−CH*$_2$−CH$_2$−CH*$_2$−P-), 2.41 (m, 6H, −P−CH$_2$−CH*$_2$−CH$_2$−P−); ^{31}P{^{1}H} NMR (101.25 MHz, CD_3NO_2) −14.0 (s); ^{19}F NMR (282.21 MHz, CH_3NO_2, coaxial tube of CF_3COOH in D_2O) −81.3 (s, 18F, OTf), −145.8 (s, 12F, F$_L$). **3a**/**3a′**: Anal. Calcd for $(C_{45}H_{34}F_{10}N_2O_6P_2PtS_2)$n (n. 1209.9): C, 44.66; H, 2.83; N, 2.31; S, 5.29. Found: C, 44.59; H, 2.82; N, 2.28; S, 5.31. ESP(+) *m*/*z*: 305 [**L**·H$^+$]$^+$, 455 [Pt(dppp)**L**]$^{2+}$, [**3a′** − 6OTf]$^{6+}$ or [**3a** − 8OTf]$^{8+}$, 656 [**3a** − 6OTf]$^{6+}$, 1059 [Pt(dppp)**L**·OTf]$^+$, [**3a** − 4OTf]$^{4+}$ or [**3a′** − 3OTf]$^{3+}$, 1364 [Pt(dppp)**L**$_2$·OTf]$^+$, 1464 [**3a** − 3OTf]$^{3+}$. IR (KBr, cm^{-1}): 1619, 1479, 985, 841 (**L**), 1438, 1107 (dppp), 1286, 1257, 1157, 1031, 639, 519 (OTf).

Square/Triangle 4a/4a′. 1,4-Bis(4-pyridyl)tetrafluorobenzene (**L**) (7 mg, 0.023 mmol) and [$Pd(dppp)(H_2O)_2$]$(OTf)_2$ (**2a**) (19 mg, 0.023 mmol) were reacted and worked up as described for **3a**/**3a′** to yield 18 mg (70%) of a brown solid. **4a**: ^{1}H NMR (250.13 MHz, CD_3NO_2,) 8.91 (d-like, J = 5.4 Hz, 16H, H$_{\alpha-py}$), 7.74−7.39 (m, 80H, Ph), 7.29 (d-like, J = 5.4 Hz, 16H, H$_{\beta-py}$), 3.25 (brs, 16H, −P−CH*$_2$−CH$_2$−CH*$_2$−P−), 2.52 (m, 8H, −P−CH$_2$−CH*$_2$−CH$_2$−P−); ^{31}P{^{1}H} NMR (101.25 MHz, CD_3NO_2) 7.7 (s); ^{19}F NMR (282.21 MHz, CH_3NO_2, coaxial tube of CF_3COOH in D_2O) −81.4 (s, 24F, OTf), −145.4 (s, 16F, F$_L$). **4a′**: ^{1}H NMR (250.13 MHz, CD_3NO_2,) 8.75 (d-like, J = 6.2 Hz, 12H, H$_{\alpha-py}$), 7.74−7.39 (m, 60H, Ph), 7.25 (d-like, J = 6.2 Hz, 12H, H$_{\beta-py}$), 3.25 (brs, 12H, −P−CH*$_2$−CH$_2$−CH*$_2$−P−), 2.52 (m, 6H, −P−CH$_2$−CH*$_2$−CH$_2$−P−); ^{31}P{^{1}H} NMR (101.25 MHz, CD_3NO_2) 8.9 (s);

(25) Andrae, D.; Haeussermann, U.; Dolg, M.; Stoll, H.; Preuss, H. *Theor. Chim. Acta* **1990**, *77*, 123−141.
(26) Kutzelnigg, W.; Fleischer, U.; Schindler, M. *NMR Basic Principles and Progress;* Berlin, 1990; Vol. 23, p 165−262.
(27) Hehre, W.; Radom, L.; Schleyer, P. R. v.; Pople, J. A. *Ab Initio Molecular Orbital Theory*; Wiley: New York, 1986.
(28) Kaupp, M.; Malkin, V. G.; Malkina, O. L.; Salahub, D. R. *Chem. Phys. Lett.* **1995**, 382−388.
(29) Kaupp, M.; Malkin, V. G.; Malkina, O. L.; Salahub, D. R. *Chem. Eur. J.* **1996**, *2*, 24−30.

(30) 4-Bromopyridine hydrochloride was treated with NaOH in H_2O. Et_2O was added, and the resulting 4-bromopyridine ethereal solution was dried over $MgSO_4$ and CaH_2 and taken to dryness under vacuum.
(31) The volume of depe must be measured very accurately by a Hamilton syringe in order to avoid the formation of [$Pt(depe)_2$][$PtCl_4$].

^{19}F NMR (282.21 MHz, CH_3NO_2, coaxial tube of CF_3COOH in D_2O) −81.4 (s, 18F, OTf), −145.9 (s, 12F, F_L). **4a**/**4a′**: Anal. Calcd for $(C_{45}H_{34}F_{10}N_2O_6P_2PdS_2)n$ (n. 1121.2): C, 48.21; H, 3.05; N, 2.50; S, 5.72. Found: C, 48.15; H, 3.07; N, 2.48; S, 5.68. ESP(+) *m*/*z*: 305 [**L**·H$^+$]$^+$, 520 [**4a′** − 5OTf]$^{5+}$, 563 [Pd(dppp)$\mathbf{L}_2$]$^{2+}$, 596 [**4a** − 6OTf]$^{6+}$, 667 [Pd(dppp)·OTf]$^+$, 972 [Pd(dppp)**L**·OTf]$^+$, [**4a** − 4OTf]$^{4+}$ or [**4a′** − 3OTf]$^{3+}$, 1347 [**4a** − 3OTf]$^{3+}$. IR (KBr, cm^{-1}): 1619, 1473, 985, 838 (**L**), 3107, 1438, 1104 (dppp), 1286, 1262, 1157, 1031, 636, 519 (OTf).

Square/Triangle 3b/3b′. Solid 1,4-bis(4-pyridyl)tetrafluorobenzene (**L**) (7 mg, 0.023 mmol) was added to a CH_2Cl_2 (6 mL) solution of [Pt(dppf)$(H_2O)_2$](OTf)$_2$ (**1b**) (25 mg, 0.023 mmol) at room temperature. After 3 h of stirring, the reaction mixture was concentrated to 3 mL under reduced pressure and an orange solid was precipitated upon addition of 4 mL of Et_2O. Filtration and drying in vacuo gave 22 mg (70%) of the product. **3b**: ^{1}H NMR (250.13 MHz, CD_3NO_2) 8.71 (d-like, J = 3.9 Hz, 16H, $H_{\alpha-py}$), 8.02−7.59 (m, 80H, Ph), 7.28 (d-like, J = 3.9 Hz, 16H, $H_{\beta-py}$), 4.80 (brs, 16H, $H_{\alpha-ferr}$), 4.73 (brs, 16H, $H_{\beta-ferr}$); ^{31}P{^{1}H} NMR (101.25 MHz, CD_3NO_2) 3.0 (s, J_{P-Pt} = 3365 Hz); ^{19}F NMR (282.21 MHz, CH_2Cl_2, coaxial tube of CF_3COOH in D_2O) −81.2 (s, 24F, OTf), −143.8 (s, 16F, F_L); ^{195}Pt{^{1}H} NMR (53.53 MHz, CD_3NO_2) −4261 (t, J_{Pt-P} = 3365 Hz). **3b′**: ^{1}H NMR (250.13 MHz, CD_3NO_2) 8.54 (d-like, J = 4.1 Hz, 12H, $H_{\alpha-py}$), 8.02−7.59 (m, 60H, Ph), 7.24 (d-like, J = 4.1 Hz, 12H, $H_{\beta-py}$), 4.85 (brs, 12H, $H_{\alpha-ferr}$), 4.73 (brs, 12H, $H_{\beta-ferr}$); ^{31}P{^{1}H} NMR (101.25 MHz, CD_3NO_2) 3.6 (s, J_{Pt-P} = 3420 Hz); ^{19}F NMR (282.21 MHz, CH_2Cl_2, coaxial tube of CF_3COOH in D_2O) −81.2 (s, 18F, OTf), −144.3 (s, 12F, F_L); ^{195}Pt{^{1}H} NMR (53.53 MHz, CD_3NO_2) −4272 (t, J_{Pt-P} = 3420 Hz). **3b**/**3b′**: Anal. Calcd for $(C_{52}H_{36}F_{10}N_2O_6FeP_2PtS_2)n$ (n. 1351.84): C, 46.20; H, 2.83; N, 2.07; S, 4.74. Found: C, 46.24; 2.81; N, 2.05; S, 4.71. ESP(+) *m*/*z*: 305 [**L**·H$^+$]$^+$, 527 [Pt(dppf)**L**]$^{2+}$, [**3b′** − 6OTf]$^{6+}$ or [**3b** − 8OTf]$^{8+}$, 623 [**3b** − 7OTf]$^{7+}$, 663 [**3b′** − 5OTf]$^{5+}$, 679 [Pt(dppf)$\mathbf{L}_2$]$^{2+}$, 865 [**3b′** − 4OTf]$^{4+}$, 898 [Pt(dppf)·OTf]$^+$, 1879 [**3b′** − 2OTf]$^{2+}$. IR (KBr, cm^{-1}): 1618, 1482, 985, 838 (**L**), 1438, 1102 (dppf), 1280, 1257, 1166, 1031, 639, 522 (OTf).

Square/Triangle 4b/4b′. 1,4-Bis(4-pyridyl)tetrafluorobenzene (**L**) (7 mg, 0.023 mmol) and [Pd (dppf)$(H_2O)_2$](OTf) (**2b**) (23 mg, 0.023 mmol) were reacted and worked up as described for **3b**/**3b′** to yield 21 mg (72%) of a violet solid. **4b**: ^{1}H NMR (250.13 MHz, CD_3NO_2) 8.68 (d-like, J = 4.6 Hz, 16H, $H_{\alpha-py}$), 8.02−7.62 (m, 80H, Ph), 7.24 (d-like, J = 4.6 Hz, 16H, $H_{\beta-py}$), 4.83 (brs, 16H, $H_{\alpha-ferr}$), 4.77 (brs, 16H, $H_{\beta-ferr}$); ^{31}P{^{1}H} NMR (101.25 MHz, CD_3NO_2) 33.6 (s); ^{19}F NMR (282.21 MHz, CH_2Cl_2, coaxial tube of CF_3COOH in D_2O) −81.2 (s, 24F, OTf), −144.2 (s, 16F, F_L). **4b′**: ^{1}H NMR (250.13 MHz, CD_3NO_2) 8.51 (d-like, J = 5.9 Hz, 12H, $H_{\alpha-py}$), 8.02−7.62 (m, 60H, Ph), 7.20 (d-like, J = 5.9 Hz, 12H, $H_{\beta-py}$), 4.86 (brs, 12H, $H_{\alpha-ferr}$), 4.77 (brs, 12H, $H_{\beta-ferr}$); ^{31}P{^{1}H} NMR (101.25 MHz, CD_3NO_2) 34.3 (s); ^{19}F NMR (282.21 MHz, CH_2Cl_2, coaxial tube of CF_3COOH in D_2O) −81.2 (s, 18F, OTf), −144.6 (s, 12F, F_L). **4b**/**4b′**: Anal. Calcd for $(C_{52}H_{36}F_{10}N_2O_6FeP_2PdS_2)n$ (n. 1263.15): C, 49.44; H, 3.03; N, 2.22; S, 5.08. Found: C, 49.39; H, 3.00; N, 2.18; S, 5.11. ESP(+) *m*/*z*: 305 [**L**·H$^+$]$^+$, 708 [Pd(dppf)$\mathbf{L}_2$·OTf·H$^+$]$^{2+}$, 808 [Pd(dppf)·OTf]$^+$, 1113 [Pd(dppf)**L**·OTf]$^+$, [**4b′** − 3OTf]$^{3+}$ or [**4b** − 4OTf]$^{4+}$, 1532 [**4b** − 3OTf]$^{3+}$. IR (KBr, cm^{-1}): 1617, 1476, 984, 830 (L), 1437, 1097 (dppf), 1279, 1257, 1165, 1030, 638, 496 (OTf).

Square/Triangle 3c/3c′. 1,4-Bis(4-pyridyl)tetrafluorobenzene (**L**) (7 mg, 0.023 mmol) and [Pt (OTf)$_2$(depe)] (**1c**) (16 mg, 0.023 mmol) were reacted and worked up as described for **3a**/**3a′** to yield 17 mg (75%) of a white solid. **3c**: ^{1}H NMR (250.13 MHz, CD_3NO_2) 9.15 (d-like, J = 5.9 Hz, 16H, $H_{\alpha-py}$), 7.95 (d-like, J = 5.9 Hz, 16H, $H_{\beta-py}$), 2.25 (m, 32H, $-CH^*_2-CH_3$), 2.06 (brs, 16 H, $-P-CH_2-CH_2-P-$), 1.31 (m, 48H, $-CH_3$); ^{31}P{^{1}H} NMR (101.25 MHz, CD_3NO_2) 44.1 (s, J_{Pt-P} = 3119 Hz); ^{19}F NMR (282.21 MHz, CH_3NO_2, coaxial tube of CF_3COOH in D_2O) −81.9 (s, 24F, OTf), −145.3 (s, 16F, F_L); ^{195}Pt {^{1}H} NMR (53.53 MHz, CD_3NO_2) −4677 (t, J_{Pt-P} = 3119 Hz). **3c′**: ^{1}H NMR (250.13 MHz, CD_3NO_2) 9.06 (d-like, J = 5.8 Hz, 12H, $H_{\alpha-py}$), 7.86 (d-like, 12H, J = 5.8 Hz, $H_{\beta-py}$), 2.25 (m, 24H, $-CH^*_2-CH_3$), 2.06 (brs, 12H, $-P-CH_2-CH_2-P-$), 1.31 (m, 36H, $-CH_3$); ^{31}P{^{1}H} NMR (101.25 MHz, CD_3NO_2) 45.2 (s, J_{P-Pt} = 3127 Hz); ^{19}F NMR (282.21 MHz, CH_3NO_2, coaxial tube of CF_3COOH in D_2O) −80.9 (s, 18F, OTf), −145.3 (s, 12F, F_L); ^{195}Pt {^{1}H} NMR (53.53 MHz, CD_3NO_2, 298K) −4696 (t, J_{Pt-P} = 3127 Hz). **3c**/**3c′**: Anal. Calcd for $(C_{28}H_{32}F_{10}N_2O_6P_2PtS_2)n$ (n. 1003.70): C, 33.51; H, 3.21; N, 2.79; S, 6.39. Found: C, 33.47; H, 3.24, N, 2.82; S, 6.36. FAB(+) *m*/*z*: 305 [**L**·H$^+$]$^+$, 371 [**3c** - 7OTf·H$^+$]$^{8+}$, 447 [**3c** − 6OTf·H$^+$]$^{7+}$, 505 [Pt(depe)$\mathbf{L}_2$]$^{2+}$, 521 [**3c** − 6OTf]$^{6+}$, 550 [Pt(depe)·OTf]$^+$, 681 [**3c** − 4OTf·H$^+$]$^{5+}$, 854 [Pt(depe)**L**·OTf]$^+$, [**3c′** − 3OTf]$^{3+}$ or [**3c** − 4OTf]$^{4+}$. IR (KBr, cm^{-1}): 1595, 1463, 980, 819 (**L**), 2966, 2931, 2875, 1630 (depe), 1262, 1173, 1034, 653 (OTf).

Square/Triangle 4c/4c′. 1,4-Bis(4-pyridyl)tetrafluorobenzene (**L**) (7 mg, 0.023 mmol) and [Pd(OTf)$_2$(depe)] (**1c**) (14 mg, 0.023 mmol) were reacted and worked up as described for **3a**/**3a′** to yield 16 mg (78%) of a white solid. **4c**: ^{1}H NMR (250.13 MHz, CD_3NO_2, 3 mM,[32] 250 K) 9.13 (m, 16H, $H_{\alpha-py}$), 7.88 (m, 16H, $H_{\beta-py}$), 2.51 (m, 16H, $-P-CH_2-CH_2-P-$), 2.28 (m, 32H, $-CH^*_2-CH_3$), 1.28 (m, 48H, $-CH_3$); ^{31}P{^{1}H} NMR (101.25 MHz, CD_3NO_2, 3 mM, 250 K) 76.0 (s); ^{19}F NMR (282.21 MHz, CD_3NO_2, 3 mM, 250K) −80.8 (s, 24F, OTf), −145.4 (s, 16F, F_L). **4c′**: ^{1}H NMR (250.13 MHz, CD_3NO_2, 3 mM, 250K) 9.05 (m, 12H, $H_{\alpha-py}$), 7.80 (m, 12H, $H_{\beta-py}$), 2.51 (m, 12H, $-P-CH_2-CH_2-P-$) 2.28 (m, 24H, $-CH^*_2-CH_3$), 1.28 (m, 36H, $-CH_3$); ^{31}P{^{1}H} NMR (101.25 MHz, CD_3NO_2, 3 mM, 250K) 77.7 (s); ^{19}F NMR (282.21 MHz, CD_3NO_2, 3 mM, 250 K) −80.8 (s, 18F, OTf) −145.3 (s, 12F, F_L). **4c**/**4c′**: Anal. Calcd for $(C_{28}H_{32}F_{10}N_2O_6P_2PdS_2)n$ (n. 915.01): C, 36.75; H, 3.52; N, 3.06; S, 7.01. Found: C, 36.67; H, 3.55; N, 3.10; S, 6.97. FAB(+) *m*/*z*: 305 [**L**·H$^+$]$^+$, 308 [Pd(depe)**L**]$^{2+}$, [**4c** − 8OTf]$^{8+}$ or [**4c′** − 6OTf]$^{6+}$, 399 [**4c′** − 5OTf]$^{5+}$, 461 [Pd(depe)·OTf]$^+$, [Pd(depe)$\mathbf{L}_2$]$^{2+}$, or [**4c** − 6OTf]$^{6+}$, 765 [Pd(depe)**L**·OTf]$^+$, [**4c** − 4OTf]$^{4+}$ or [**4c′** − 3OTf]$^{3+}$, 1073 [Pd(depe)$\mathbf{L}_2$·OTf]$^+$ or [**4c** − 3OTf]$^{3+}$. IR (KBr, cm^{-1}): 1599, 1464, 981, 820 (**L**), 2959, 2931, 2903, 2868 (depe), 1261, 1173, 1034, 652, 519 (OTf).

Crystal Structure Analysis of *cis*-[PtCl$_2$(depe)] and *cis*-[Pd(dppf)$(H_2O)_2$](CF$_3$SO$_3$)$_2$ (2b).[33] Data collection were carried out at 298(2) K on a Bruker SMART-CCD area diffractometer with graphite-monochromated Mo Kα radiation (λ = 0.71073 Å) operating at 50 kV and 30 mA. Suitable single crystals of *cis*-[PtCl$_2$(depe)] (block, colorless, 0.50 × 0.20 × 0.16 mm^3) and **2b** (block, dark green, 0.26 × 0.21 × 0.06 mm^3) were used for crystal determination. A total of 1271 frames of intensity data were collected over a hemisphere of the reciprocal space by combination of three exposure sets. Each frame covered 0.3° in ω, and the first 50 frames were re-collected at the end of data collection to monitor crystal decay. The integration process yields a total of 8421 reflections of which 3194 were independent [R(int) = 0.0407] for *cis*-[PtCl$_2$(depe)] and a total of 23071 reflections of which 8119 were independent [R(int) = 0.0548] for **2b**. Absorption corrections

(32) The molarity is based on the number of moles of palladium.

(33) Crystallographic data (excluding structure factors) have been deposited with the Cambridge Crystallographic Data Centre as deposition numbers CCDC-206244 (compound *cis*-[PtCl$_2$(depe)]) and CCDC-206245 (compound **2b**). Copies of the data can be obtained, free of charge, on application to the CCDC, 12 Union Road, Cambridge CB2 1EZ U.K. [fax, +44(1223)336033; e-mail, deposit@ccdc.cam.ac.uk].

were applied using the SADABS program[34] (maximum and minimum transmission coefficients, 0.3137 and 0.0883 for *cis*-[$PtCl_2$(depe)] and 0.9380 and 0.7666 for **2b**). The structure was solved using the *Bruker SHELXTL-PC* software[35] by direct methods and refined by full-matrix least-squares methods on F^2. Hydrogen atoms were included in calculated positions, less those of water molecules that were located on residual density maps, but then fixed their positions, and refined in the riding mode. The details of the data collection and refinement are summarized in Table 1 (Supporting Information).

Results and Discussion

Preparation and Characterization of Metallacycles. Our initial goal was the construction of molecular polygons via *cis*-protected Pd(II) and Pt(II) phosphane triflates and the new diaza ligand **L**. The preparation of the corner units involves reaction of the transition metal halide with silver triflate in the appropriate organic solvent. Stang et al.[1a] introduced the *cis*-dpppPd(II) and *cis*-dpppPt(II) units, and, although preferentially these complexes form molecular squares with linear diaza ligands, very recently, equilibria between molecular triangles and squares have been reported[10g] and exhaustively studied by mass spectrometry.[36] *cis*-dppfPd(II) and its platinum analogues were successfully used for the synthesis of octanuclear square-shaped metallomacrocycles.[16] Finally, *cis*-depePd(II) or *cis*-depePt(II) corners have been employed in this work for the first time. In order to ascertain the suitability of *cis*-depeM(II) metal corners for the preparation of molecular squares and triangles and determine the structural differences between the palladium and platinum units *cis*-dppfM(II), which potentially could be able to lead to macromolecules of different geometry, we undertook the X-ray analysis of *cis*-[$PtCl_2$(depe)] and *cis*-[Pd(dppf)(H_2O)$_2$](OTf)$_2$ (see Supporting Information).

The incorporation of tetrafluorophenylene units as part of the bridging linkers provides self-assembled electron-poor cavities that show molecular recognition ability for electron-rich aromatic compounds.[6c,10b,37] However, due to the flexibility of the tested fluorinated derivatives (pyCH_2(C_6F_4)$_n$-CH_2py: $n = 1, 2$), it has only been possible to obtain either dinuclear or polymeric species so far. To achieve the preparation of molecular polygons, we designed and prepared the rigid fluorinated ligand 1,4-bis(4-pyridyl)tetrafluorobenzene (**L**). This new organic ligand was synthesized in moderate yield (ca. 40%) by a palladium-catalyzed cross-coupling reaction[38] between the Grignard reagent 1,4-dibromotetrafluorophenyldimagnesium and 2 equiv of 4-bromopyridine (Scheme 1). Alternatively, the same compound can be obtained by a [$PdCl_2$(PPh_3)$_2$]/LiCl-promoted cross-coupling reaction[39] between 2 equiv of 4-pyridyltrimethylstannane and 1,4-dibromotetrafluorobenzene with similar yields. The compound was characterized by elemental analyses and ^{1}H, ^{13}C, and ^{19}F NMR and IR spectroscopies. EMS supported the molecular mass of **L**: *m*/*z* 304.

Scheme 1

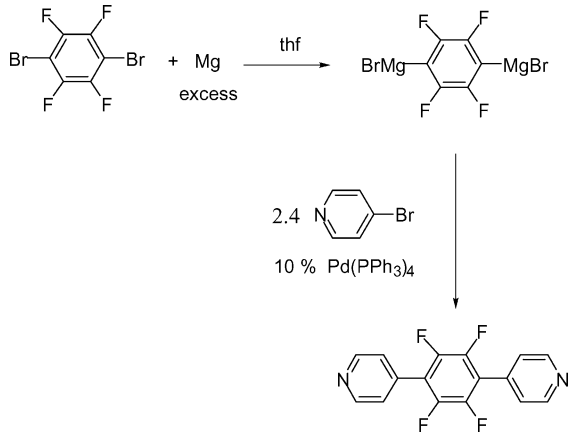

Stoichiometric amounts of *cis*-[Pt(dppp)(H_2O)$_2$](OTf)$_2$ (**1a**), *cis*-[Pt(dppf)(H_2O)$_2$](OTf)$_2$ (**1b**), or *cis*-[Pt(OTf)$_2$(depe)] (**1c**) and the bidentate ligand **L** were treated in dichloromethane (**1b**) or nitromethane (**1a**, **1c**) at room temperature to yield on mixing solutions whose NMR multinuclear spectra showed the assemblies of two main components with highly symmetric structures (Scheme 2). No signals attributable to the starting materials were detected. Reactions with the analogous palladium units **2a**, **2b**, or **2c** gave similar results.

In order to clarify our results, we will discuss the experiences separately. The reaction of *cis*-[Pd(dppf)(H_2O)$_2$]-(OTf)$_2$ compound **2b** and **L** gave a violet dichloromethane solution whose ^{31}P{^{1}H}NMR spectrum showed two signals at 33.2 (major intensity) and 32.6 ppm. The observed upfield shifts from the precursor are in agreement with an aza-ligand coordination.[15] In the ^{19}F NMR spectrum appeared two resonances at −144.2 (minor intensity) and −144.6 ppm which were shifted downfield about 2 ppm from the peak at −146.4 ppm of **L**. The ^{1}H NMR spectrum corroborated the existence of the two macrocyclic species since it showed two sets of resonances for H_α (8.54, 8.51 ppm) and H_β (7.24, 7.21 ppm) protons of the pyridine rings. Four signals for the protons of the Cp rings could be seen as well. The three NMR spectra presented identical integration ratios between the signals corresponding to both components for a given concentration. In this case, the major component was assigned to the triangular molecular species (**4b′**) while the minor component was assigned to the square species (**4b**). This assignment is strongly supported by the concentration effects on the equilibrium ratio studied in dichloromethane: the signal intensity in the ^{31}P{^{1}H} NMR spectrum of the minor component (**4b**) increases at higher concentrations

(34) Sheldrick, G. M. *SADABS. A Program for Empirical Absorption Correction of Area Detector Data;* University of Göttingen: Göttingen, Germany, 1996.
(35) (a) Sheldrick, G. M. *SHELXS-97, A Program for Solving Crystal Structures*; University of Göttingen: Göttingen, Germany, 1997. (b) Sheldrick, G. M. *SHELXL-97, A Program for Crystal Structure Refinement*; University of Göttingen: Göttingen, Germany, 1997.
(36) Schalley, C. A.; Muller, T.; Linnartz, P.; Witt, M.; Schäfer, M.; Lützen, A. *Chem. Eur. J.* **2002**, *8*, 3538−3538.
(37) Kasai, K.; Aoyagi, M.; Fujita, M. *J. Am. Chem. Soc.* **2000**, *122*, 2140−2141.
(38) Amatore, C.; Jutand, A.; Negri, S.; Fauvarque, J.-F. *J. Organomet. Chem.* **1990**, *390*, 389−398.
(39) Fujita, M.; Oka, H.; Ogura, K. *Tetrahedron Lett.* **1995**, *36*, 5247−5250.

Scheme 2

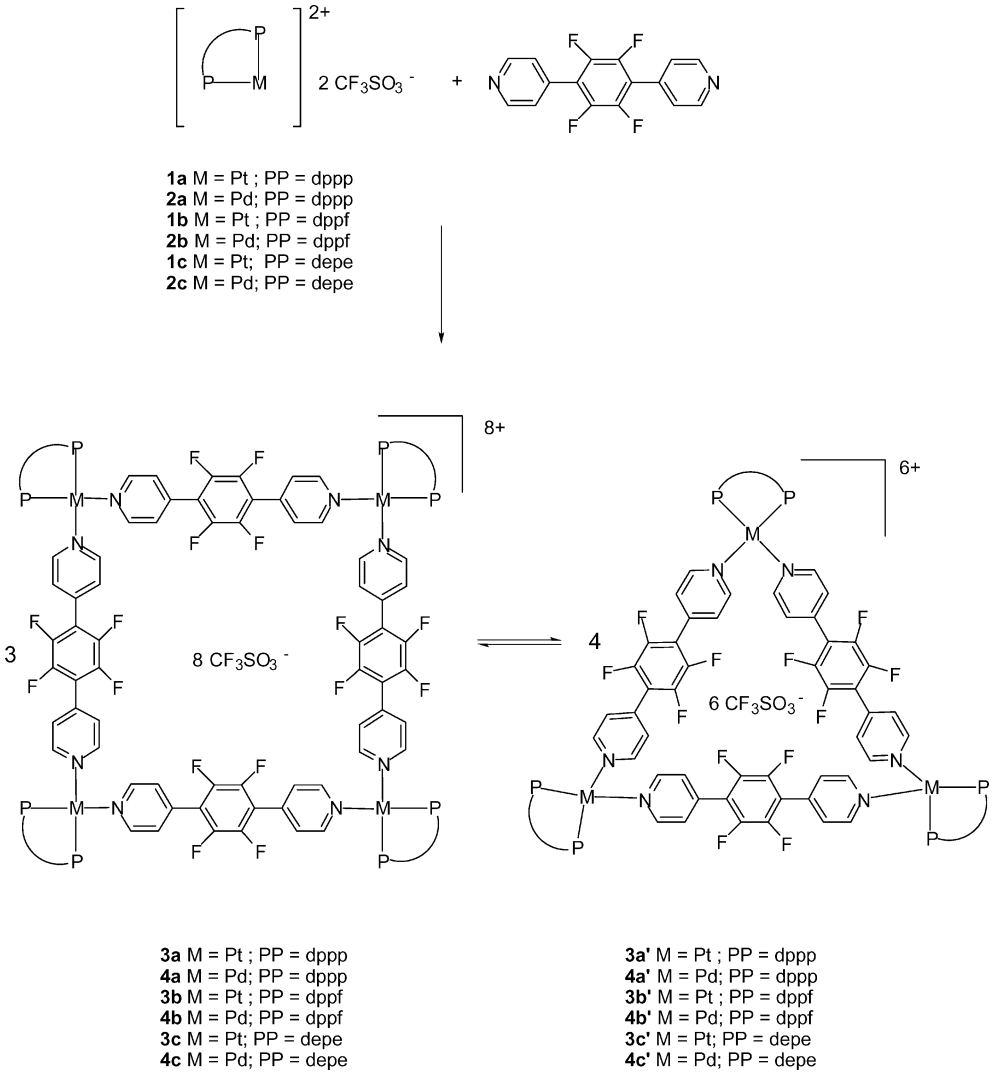

(Figure 1) while that of the major component (**4b′**) decreases according to Le Chatelier's law. Moreover, the relative position of NMR peaks for both triangle and square is in agreement with previous observations pointed out by Schalley et al.[36] Thus, the signals in the ^{1}H NMR spectrum of the protons *ortho* to the pyridyl-nitrogen atom of the square **4b** are observed downfield compared to those of the triangle **4b′** while, in the corresponding ^{31}P{^{1}H} NMR spectrum, the resonance due to **4b** appears upfield. Similar trends can be deduced from the observation of the ^{19}F NMR spectra where the signals of the triangles appeared at lower frequencies than those of the squares. In order to confirm the observed trends in the chemical shift between triangular and square macrocycles, a GIAO-DFT study was carried out (see below).

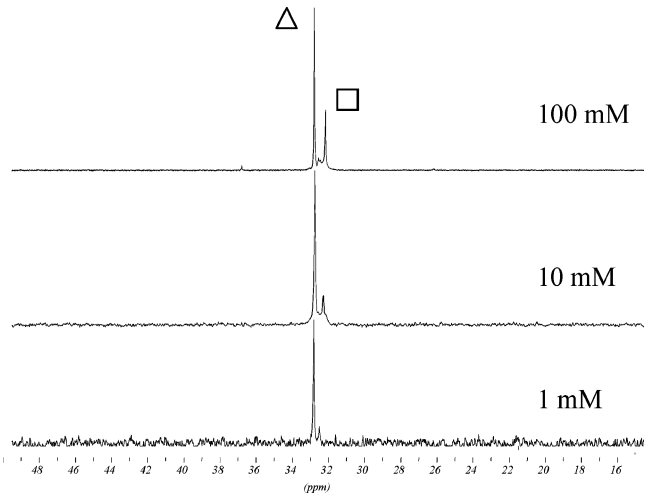

Figure 1. ^{31}P{^{1}H} NMR spectra of **4b**/**4b′** at different concentrations in CH_2Cl_2 solution.

It is worth noting that the molecular **4b**/**4b′** system provides an interesting example of the decisive role of the solvents in shifting the square/triangle equilibrium. Indeed, its ^{31}P{^{1}H} NMR spectrum in acetone-d_6 showed, in contrast to that exhibited in dichloromethane, a unique peak at 36.0 ppm. The ^{1}H NMR spectrum displayed only a set of signals due either to the pyridyl moiety or to Cp rings. These signals are reasonably assigned to the triangular component, which was the predominant species in dichloromethane, as discussed above. Unfortunately, the mass spectrum was not informative and, although several attempts of growing crystals were made, no good-quality single crystals could

be obtained that would support this assignment. The NMR spectra (including $^{195}Pt\{^1H\}$NMR) of solutions of the analogous platinum compounds (**3b**/**3b′**) featured similar characteristics; however, in this case, the square/triangle ratio is much more shifted toward the latter component (equilibrium ratio greater than 1:10 in the range of studied concentrations).

The results obtained in the reaction of **1a** or **2a** with **L** contrast with those described above. The analysis of the NMR spectra of the solutions of compounds containing dppp as auxiliary ligand, **3a**/**3a′** and **4a**/**4a′**, confirmed that the square form, assigned by means of mass spectrometry and NMR multinuclear studies on solutions at different concentrations, clearly predominates over the triangular one. In this case, the comparative study of the square/triangle ratio in different solvents could not be carried out given the insolubility of these macromolecules in the majority of common organic solvents.

Although reasons for the different behavior of both types of complexes are unclear as yet, the flexibility and/or the bite angle of the bidentate ligands seem to play an important role. Thus, dppf (bite angle 98.74°)[40] would facilitate the formation of N−M−N angles suitable for triangular assemblies while it would be more difficult for this to occur for the more rigid dppp ligand (bite angle 91.56°).[40] However, examples in the literature do not support this idea: the self-assembly of the dppf derivatives **1b** or **2b** with 2,7-diazapyrene and 4,4′-azopyridine is reported to result in the formation of square molecules.[16]

In order to test whether the value of the diphosphine bite angle would have an influence on the formation of the square and/or triangular assemblies, we prepared the depe derivatives **1c** and **2c**. The fact that depe had a smaller bite angle (see Supporting Information) than either dppp or dppf together with the sterically less demanding backbone of depe would, from a thermodynamic point of view, favor the formation of the square versus the triangle. Nevertheless, the results were different from what was expected. The $^{31}P\{^1H\}$ NMR spectrum of the solution obtained on mixing equimolar quantities of *cis*-[Pt(OTf)$_2$(depe)] (**1c**) and **L** in nitromethane showed two singlets (44.1 and 45.2 ppm) whose relative intensity varied drastically as a function of concentration; that is, at low concentrations the predominant species was seen to be the triangle **3c′** ($\delta(^{31}P) = 45.2$ ppm) while at high concentrations the square **3c** ($\delta(^{31}P) = 44.1$ ppm) was the most abundant. The same variation in the ratio square/triangle was observed in ^1H, ^{19}F, and $^{195}Pt\{^1H\}$ NMR spectra.

For palladium (**2c** and **L** 1:1 in nitromethane), room temperature NMR experiments implied dynamic processes on the NMR scale. Therefore, variable temperature spectra for a given concentration (3 mM) were recorded over the temperature range 250−333 K (Figure 2). Above 298 K the $^{31}P\{^1H\}$ NMR spectra recorded in deuterated nitromethane only showed a very broad resonance at 78 ppm. Between

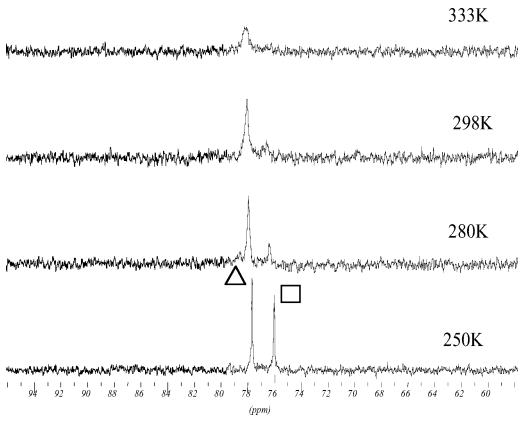

Figure 2. Variable temperature $^{31}P\{^1H\}$ NMR spectra in CD_3NO_2 for **4c**/**4c′**.

250 and 298 K the spectra displayed two singlets (77.9 and 76.4 ppm) that sharpen notably at lower temperatures. The integral ratio between the two peaks did not present significant variations with the temperature, the triangle **4c′** being prevalent. Analogously to the platinum compounds, an inversion of this ratio was observed and square **4c** showed itself to be the most abundant entity at high concentrations.

Computer Modeling. A theoretical study using force field methods to determine the relative stability of the platinum compounds with dppf (**3b**/**3b′**) was performed with the Cerius2 program package (see Computational Details section). The conformers with the lowest energy are represented in Figure 3. The bite angle of the diphosphine ligand is similar in both compounds with values around 95−96° while the N−Pt−N angle is approximately 2° larger in the case of the square compound. The analysis of the relative stability of compounds **3b** and **3b′** using force field methods indicates a lower energy for the square compound **3b**, around 5 kcal/mol per edge. This fact can be understood by looking at the molecular models of Figure 3 where clearly in the triangular compound an extra energy contribution is needed to bend the 1,4-bis(4-pyridyl)tetrafluorobenzene ligand. Also, triangular complexes show a larger steric hindrance between the bridging ligands. However, as pointed out previously, NMR results indicate the predominance of the triangular compound **3b′**. This predominance is probably due to the kinetic control of the reaction process, since the square compound **3b** is considered as the thermodynamically favored product. It is worth noting that a stable complex with a butterfly shape (S_4 symmetry) was found during the conformer search, however, there is not experimental evidence of the existence of such systems.

In order to evaluate the influence of the bite angle of the diphosphine in the relative stability of the triangular and square compounds, we extended our study to the dppp complexes (**3a** and **3a′**, see Figure 4). The phosphine bite angles of the optimized structure follow the same trend as in the experimental data and are around 3° smaller than those corresponding to the compounds with the dppf ligand. The comparison of the N−Pt−N angle value shows, as the main difference between both ligands, an increase of this angle value with the dppp for the triangular compound (**3a′**) while there are no appreciable changes between the angles of the

(40) Dierkes, P.; Van Leeuven, P. W. N. M. *J. Chem. Soc., Dalton Trans.* **1999**, 1519−1530.

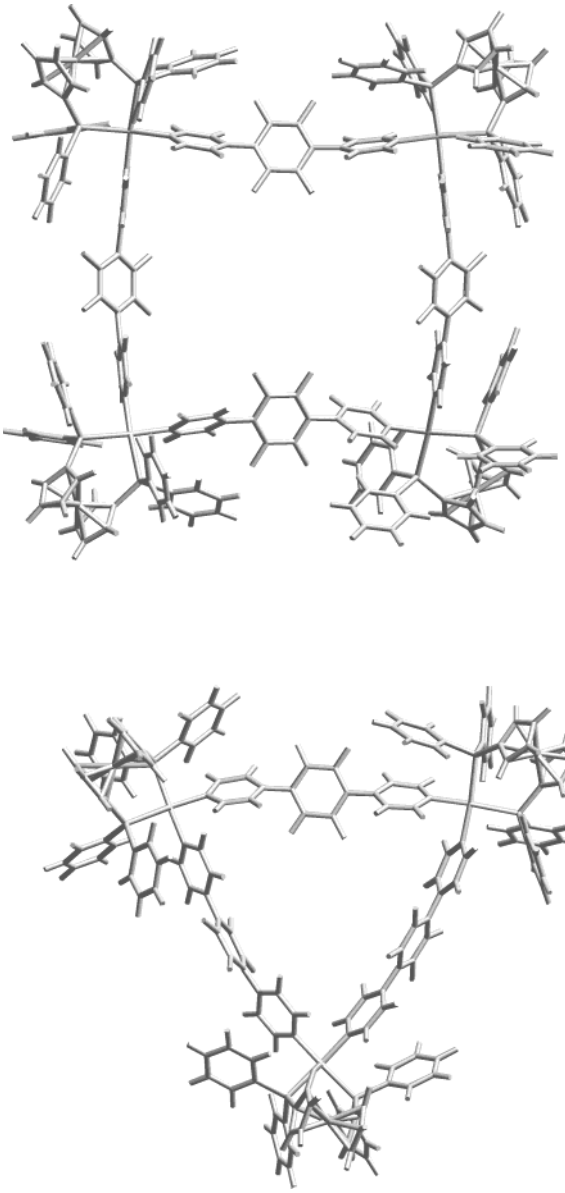

Figure 3. Optimized structures corresponding to the **3b** and **3b′** compounds (dppf ligand) obtained using the universal force field as implemented in the Cerius2 package.

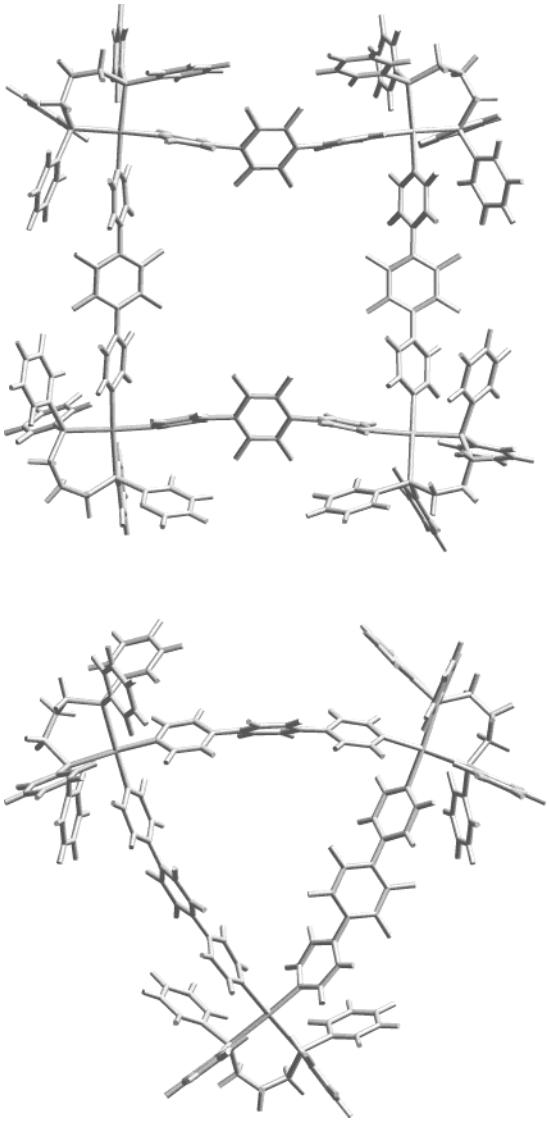

Figure 4. Optimized structures corresponding to the **3a** and **3a′** compounds (dppp ligand) obtained using the universal force field as implemented in the Cerius2 package.

square compounds. The increase of the N−Pt−N angle produces a larger bending of the ligand **L**, and this implies a larger relative stability of the square compound (**3a**) (around 11 kcal/mol per edge in comparison with the triangular complexes). This value is almost twice that found for the compounds with the dppf ligand. This fact agrees well with the predominance of the square compound with dppp ligand (**3a**) found in the NMR data. However, similar analysis for depe complexes does not show a clear tendency of the relative stability with the diphosphine bite angle since, although the depe complexes present a smaller bite angle, the energy difference is only of 3 kcal/mol par edge favorable to the square complex. This result would justify the observed inversion of the square/triangle ratio on varying concentrations.

Determination of Chemical Shifts by GIAO-DFT Calculations. In order to confirm the changes in the chemical shift between the triangular complexes and the square complexes, we performed a GIAO-DFT study (see Computational Details section).[41,42] For the comparison, we selected the only example reported by Stang et al. where both structures were resolved by X-ray diffraction.[11] These complexes are obtained using trimethylphosphine as terminal ligand while the bridging ligand is *trans*-bis(4-pyridyl)-ethylene. Due to the large size of such complexes, we have employed a simplified model corresponding to a corner of the molecule (see Figure 5) to analyze the NMR shifts.

The analysis of the structure of the triangular and square complexes shows small differences, the P−Pt−P angles being almost the same in both cases (around 95°) while the N−Pt−N is slightly different (close to 82° for the triangular structure and 87° for the square complex). The GIAO results indicate an average downfield shift of the protons *ortho* to

(41) Jensen, F. *Introduction to Computational Chemistry*; J. Wiley & Sons: Chichester, 1999.
(42) Koch, W.; Holthausen, M. C. *A Chemist's Guide to Density Functional Theory*; Wiley-VCH Verlag: Weinheim, 2000.

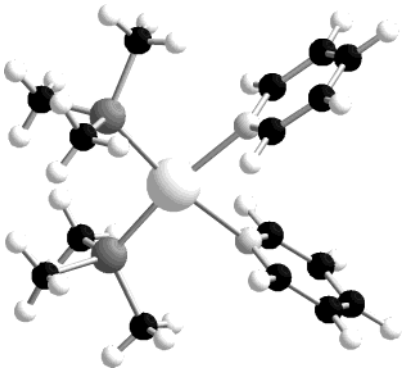

Figure 5. Molecular model employed in the GIAO-DFT calculations. The structure corresponds to a corner of the triangular and square Pt(II) complexes obtained by Stang et al. with trimethylphosphine and *trans*-bis(4-pyridyl)ethylene ligands.[11]

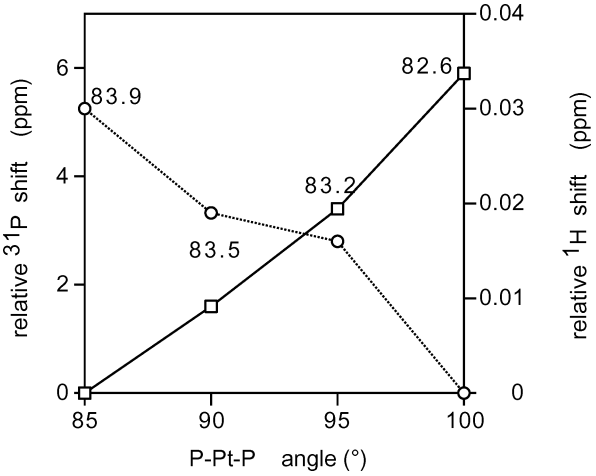

Figure 6. Calculated GIAO values for the model complex (see Figure 5) corresponding to the relative ^{31}P NMR shifts of the phosphine (squares) and ^{1}H NMR shifts of protons *ortho* to the pyridyl-nitrogen atom (circles). Optimized N−Pt−N angle values in degrees are indicated in the figure for each P−Pt−P angle considered.

the pyridyl-nitrogen atom of 0.24 ppm in the square complex, in good agreement with the downfield shift of 0.09 ppm found in Stang's compounds and those corresponding to the platinum complexes of this work, which range between 0.09 and 0.17 ppm. The opposite trend found experimentally for the ^{31}P NMR values is also reproduced with the GIAO calculations, with a calculated upfield shift of 1.6 ppm for the square complex. In our compounds, changes in shift values between 0.8 and 1.1 ppm are found from square to triangular complexes. These results also agree with those found experimentally by Schalley[36] and Würthner[10g] for similar complexes. The same study using the GIAO method for the analogous Pd complexes displays the same trends, with an average downfield shift for the square complex of 0.26 ppm for the protons *ortho* to the pyridyl-nitrogen atom and an average upfield shift of 1.4 ppm in the case of ^{31}P NMR.

In order to analyze the influence of the geometry on the chemical shift, we employed the model shown in Figure 5 by fixing the P−Pt−P angle, performing the optimization of the structure, and calculating the chemical shift for the optimized structure. Thus, we calculated the displacement corresponding to four P−Pt−P angles, and the results are shown in Figure 6. For the smaller P−Pt−P angle values, as expected, we found the larger N−Pt−N optimized angle. This case will correspond to a situation closer to a hypothetical square complex. The calculated shifts show an upfield displacement of the ^{31}P NMR values when the P−Pt−P angle diminishes, showing the opposite behavior to the ^{1}H NMR shifts. Notably, there is little dependence of the optimized N−Pt−N angle on the change of the P−Pt−P angle. These results for the NMR data confirm the trends found previously for the nonoptimized corner complexes.

A detailed analysis of the diamagnetic and paramagnetic contributions to the chemical shifts reveals that the changes indicated in Figure 6 are mainly due to the paramagnetic contribution. The paramagnetic component is inversely proportional to the gap between occupied and virtual orbitals.[43] For this system, the coupling through the magnetic operator is possible for the π-bonding orbitals of the phosphines and the virtual orbital corresponding to the combination of the $d_{x^2-y^2}$ (Pt) and σ orbitals of the phosphines (see ref 43 for a detailed example of the effect of the magnetic operator). The gap value between such orbitals decreases inversely with the P−Pt−P angle (mainly due to the virtual orbital). The analysis of the NBO populations[44] also indicates a decrease of the phosphorus electron density for larger P−Pt−P angles, giving a larger deshielding and, consequently, a larger chemical shift, as expected from the results of Figure 6.

Conclusions

From all these experiments and others reported in the literature, we conclude that it is still very difficult for the composition of the equilibrium between molecular squares and triangles to be predictable in a straightforward way. Factors such as the rigidity of the building blocks, the value of the angle of the adjacent coordination sites, and the lability of the metal−pyridine bond have to be considered responsible for driving the self-assembly process to completion. Further synthetic and theoretical studies are necessary in order to fully understand all the factors that govern the generation of one determinate entity in self-assembly reactions. The force field study of the relative stability of the square and triangular complexes does not show a clear relationship between the bite angle of the diphosphine and the stability order. These results indicate a larger stability of square complexes, suggesting that the predominance for triangular complexes found experimentally in some cases could be due to a kinetic control of the reaction. The GIAO-DFT study carried out with a model corner complex corroborates the experimental NMR data, showing an upfield shift of the ^{31}P NMR values from the triangular structures to the square ones, while the opposite behavior is found for the ^{1}H NMR shifts corresponding to protons *ortho* to the pyridyl-nitrogen atom.

(43) Ruiz-Morales, Y.; Ziegler, T. *J. Phys. Chem. A* **1998**, *102*, 3970−3976.

(44) Reed, A. E.; Curtiss, L. A.; Weinhold, F. *Chem. Rev.* **1988**, *88*, 899−926.

Acknowledgment. This work was supported by the DGICYT (Project BQU2000-0644) and the CIRIT (Project 1999 SGR 00045). M.M. is indebted to the Universitat de Barcelona for a scholarship. The computing resources were generously made available in the Centre de Computació de Catalunya (CESCA) with a grant provided by the Fundació Catalana per a la Recerca (FCR) and the Universitat de Barcelona.

Supporting Information Available: Descriptions of X-ray crystal structures (tables and figures) and X-ray crystallographic files for compounds *cis*-[$PtCl_2$(depe)] and **2b** (CIF format); electrochemical data for dppf compounds and host−guest studies. This material is available free of charge via the Internet at http://pubs.acs.org.

IC034489J